

**Spin-modulated quasi-one-dimensional antiferromagnet LiCuVO<sub>4</sub>**

N. Büttgen\* and H.-A. Krug von Nidda

*Center for Electronic Correlations and Magnetism EKM, Experimentalphysik V, Universität Augsburg, D-86135 Augsburg, Germany*

L. E. Svistov and L. A. Prozorova

*P.L. Kapitza Institute for Physical Problems, RAS, 119334 Moscow, Russia*

A. Prokofiev† and W. Aßmus

*Physikalisches Institut, Johann-Wolfgang-Goethe-Universität, D-60054 Frankfurt, Germany*

(Received 22 December 2006; revised manuscript received 31 May 2007; published 31 July 2007)

We report on magnetic resonance studies within the magnetically ordered phase of the quasi-one-dimensional antiferromagnet LiCuVO<sub>4</sub>. Our studies reveal a spin reorientational transition at a magnetic field  $H_{c1} \approx 25$  kOe applied within the crystallographic **ab** plane in addition to the recently observed one at  $H_{c2} \approx 75$  kOe [M. G. Banks *et al.*, J. Phys.: Condens. Matter **19**, 145227 (2007)]. Spectra of the antiferromagnetic resonance along low-frequency branches can be described in the framework of a macroscopic theory of exchange-rigid planar magnetic structures. These data allow us to obtain the parameter of the anisotropy of the exchange susceptibility together with a constant of the uniaxial anisotropy. Spectra of <sup>7</sup>Li nuclear magnetic resonance (NMR) show that, within the magnetically ordered phase of LiCuVO<sub>4</sub> in the low-field range  $H < H_{c1}$ , a planar spiral spin structure is realized with the spins lying in the **ab** plane, in agreement with neutron-scattering studies of Gibson *et al.* [Physica B **350**, 253 (2004)]. Based on NMR spectra simulations, the transition at  $H_{c1}$  can well be described as a spin-flop transition, where the spin plane of the magnetically ordered structure rotates to be perpendicular to the direction of the applied magnetic field. For  $H > H_{c2} \approx 75$  kOe, our NMR spectra simulations show that the magnetically ordered structure exhibits a modulation of the spin projections along the direction of the applied magnetic field  $H$ .

DOI: [10.1103/PhysRevB.76.014440](https://doi.org/10.1103/PhysRevB.76.014440)

PACS number(s): 75.50.Ee, 76.60.-k, 76.50.+g, 75.10.Pq

**I. INTRODUCTION**

The investigation of the magnetism in LiCuVO<sub>4</sub> has a long history which started with the discovery of the low dimensionality of the magnetic subsystem. This low dimensionality manifested itself in the temperature dependence of the magnetic susceptibility.<sup>1</sup> Later on, the interest was focused on the quasi-one-dimensionality of the Cu<sup>2+</sup> ( $3d^9$  configuration,  $S=1/2$ ) spin system at elevated temperatures, where three-dimensional (3D) correlations can be neglected. Intense experimental investigations on polycrystalline material have been explained in the framework of strong antiferromagnetic exchange interactions between neighboring spins along the chain of copper ions. Recent low-temperature neutron-scattering experiments have shown that there is a frustration along the chain due to the competition of the exchange interactions between nearest and next-nearest neighbors.<sup>2,3</sup> This motivated us to start a closer inspection of the magnetic properties in the low-temperature range. The hierarchy of the exchange interactions in LiCuVO<sub>4</sub> (Ref. 3) shows that the system of exchange interactions in the magnetically long-range ordered phase can be compared, from many points of view, to the quasi-two-dimensional triangular antiferromagnets with distorted lattices such as Cs<sub>2</sub>CuCl<sub>4</sub> and Cs<sub>2</sub>CuBr<sub>4</sub> (Refs. 4 and 5, respectively). In those works, the quantum and thermal fluctuations turned out to play an important role in stabilizing the particular magnetic states. Therefore, the establishment of the entire magnetic phase diagram of single crystalline LiCuVO<sub>4</sub> will be the objective of future work. In addition to the interest in the magnetic phase diagram itself, the kind of spiral-magnetic structure,

which is realized in LiCuVO<sub>4</sub> (Ref. 2), was promising to yield ferroelectricity.<sup>6</sup> Indeed, a ferroelectric transition has recently been found.<sup>7</sup>

The quasi-one-dimensionality of the spin system in LiCuVO<sub>4</sub> is provided by the magnetic ions of Cu<sup>2+</sup>. Lithium and copper ions share the octahedral sites in the orthorhombically distorted spinel structure in such a way that the copper ions are arranged in chains along the crystallographic **b** axis separated by the nonmagnetic ions of lithium, vanadium, and oxygen. The temperature dependence of the magnetic susceptibility exhibits a broad maximum around  $T = 28$  K, typical for low-dimensional antiferromagnets, and a sharp anomaly at  $T = 2.3$  K, which is associated with the establishment of 3D magnetic order. From the values of these temperatures, the authors of Ref. 8 evaluated the intrachain and interchain exchange integrals of 22.5 and 1 K, respectively. Elastic neutron-diffraction experiments<sup>2</sup> on single crystals of LiCuVO<sub>4</sub> revealed that the 3D ordered phase exhibits an incommensurate, noncollinear magnetic structure. The scheme of this suggested magnetic structure is shown in Fig. 1. According to that work,<sup>2</sup> the wave vector of this magnetic structure is directed along the copper chains ( $\mathbf{k}_{ic} \parallel \mathbf{b}$ ) and the value of the ordered magnetic moments of the Cu<sup>2+</sup> ions amounts to  $0.31 \mu_B$ , lying within the **ab** planes. The investigation of magnetic excitations in LiCuVO<sub>4</sub>, using inelastic neutron-diffraction experiments,<sup>3</sup> confirmed the quasi-one-dimensional (quasi-1D) nature of this compound and brought to conclusion that the magnetic incommensurate structure is due to an exotic ratio of intrachain exchange integrals: the nearest-neighbor exchange integral ( $J_1 = -18$  K) is ferromagnetic and it is strongly dominated by

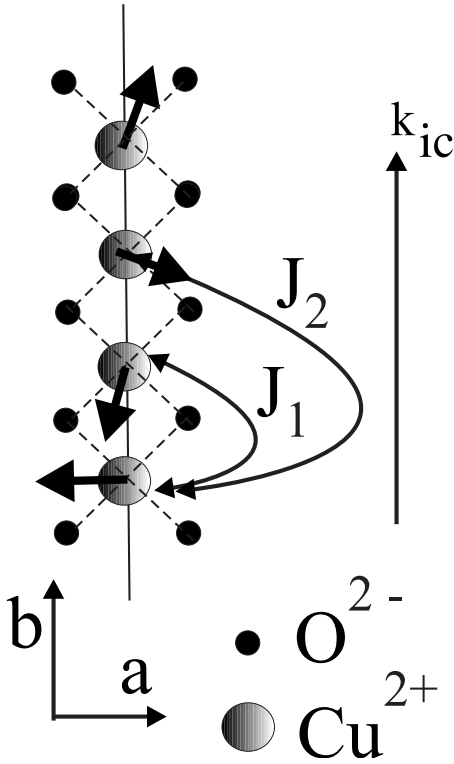


FIG. 1. Scheme of the spiral-magnetic structure of  $\text{LiCuVO}_4$  (Ref. 2). A fragment of one single chain of edge-sharing  $\text{CuO}_4$  units along with the dominant intrachain exchange integrals  $J_1$  and  $J_2$  is shown.

the value of the next-nearest exchange integral which is antiferromagnetic ( $J_2=49$  K, cf. Fig. 1). This unusual hierarchy of exchange integrals is realized in  $\text{LiCuVO}_4$  due to indirect exchange interaction through the oxygen neighborhood, and it can be explained from the Goodenough-Kanamori-Anderson rules.<sup>9</sup> Results of electron-band structure calculations give the values of the exchange integrals  $J_1$  and  $J_2$  in a good agreement with the values obtained experimentally.<sup>3</sup>

The magnetic properties of such exchange-bonded chains of Heisenberg spins with two exchange integrals  $J_1$  and  $J_2$  are similar to the so-called zigzag model where pairs of chains, with an intrachain exchange integral  $J_1$ , are coupled via an interchain exchange integral  $J_2$ . Such a model was studied theoretically in the limit of large spin values, as well as for  $S=1/2$  in Ref. 10 and 11. In these works, it was shown that such a ratio of the exchange integrals, which are obtained for  $\text{LiCuVO}_4$ , results in an incommensurate magnetic structure. The value of the incommensurate vector  $\mathbf{k}_{ic}$  experimentally obtained<sup>2</sup> is found to be between the theoretical values in the limit of large spin and for  $S=1/2$  (cf. Ref. 11).

Thus,  $\text{LiCuVO}_4$  presents an example of a quasi-1D frustrated antiferromagnet of spins  $S=1/2$ , where strong exchange interactions yield an incommensurate noncollinear magnetically ordered structure for temperatures  $T < 2.3$  K. In the present work, antiferromagnetic resonance (AFMR) and nuclear magnetic resonance (NMR) on the nuclei of non-magnetic ions ( ${}^7\text{Li}$  and  ${}^{51}\text{V}$ ) were studied for temperatures within this magnetically ordered phase. Additionally, the AFMR experiment is extended toward elevated temperatures

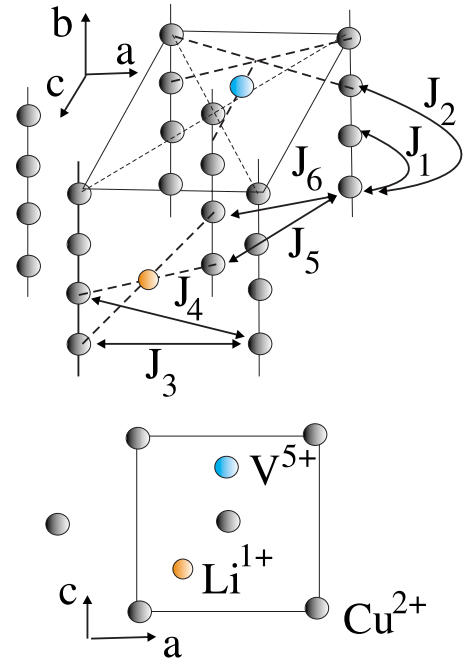


FIG. 2. (Color) Scheme of the  $\text{Cu}^{2+}$  sites in the crystal structure of  $\text{LiCuVO}_4$ . The sites of  $\text{Cu}^{2+}$  ions are marked by gray circles. One of the lithium ions is marked by an orange circle and one of the vanadium ions by a blue circle, respectively. Upper panel:  $J_1, \dots, J_6$  denote the main exchange integrals defining the magnetic structure of  $\text{LiCuVO}_4$  (Ref. 3). Lower panel: projection of the crystallographic structure on the  $ac$  plane.

$T < 30$  K, where 3D order is already absent but spin correlations along copper chains are well developed. These temperatures are within the range between the maxima of the temperature dependent magnetic susceptibility  $\chi(T)$  (cf. Fig. 4).

## II. SAMPLE PREPARATION AND EXPERIMENTAL DETAILS

$\text{LiCuVO}_4$  crystallizes in an inverse spinel structure  $AB_2O_4$  with an orthorhombic distortion stipulated by a cooperative Jahn-Teller effect, induced by  $\text{Cu}^{2+}$  ions. The crystal structure of  $\text{LiCuVO}_4$  is described by space group  $Imma$  (Refs. 12 and 13). In Fig. 2, a scheme of the crystal structure of  $\text{LiCuVO}_4$  is shown. The  $\text{Cu}^{2+}$  ions, which compose strongly exchange interacting magnetic chains, are marked with gray circles. For clearness, these copper chains along the crystallographic  $\mathbf{b}$  direction are joined with a solid line to guide the eyes.  $\text{Li}^{1+}$  ions occupy octahedrally coordinated crystallographic equivalent sites and one of the lithium ions is marked by an orange circle.  $\text{V}^{5+}$  ions occupy the tetrahedrally coordinated crystallographic equivalent sites and one of the vanadium ions is denoted by a blue circle. The lattice parameters in  $\mathbf{a}$  and  $\mathbf{c}$  directions coincide with the distance between nearest copper neighbors, but along the  $\mathbf{b}$  direction, the lattice parameter equals twice the distance between nearest copper neighbors.

Single crystals with the volume of some cubic millimeters were grown as described in detail in Ref. 12. As the ionic

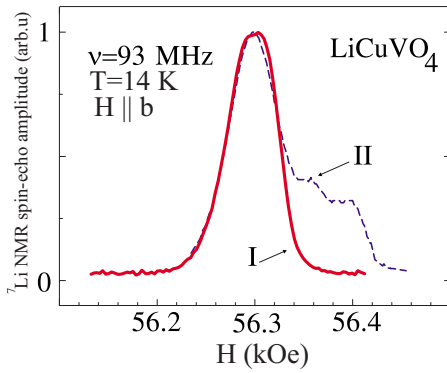


FIG. 3. (Color)  $^7\text{Li}$  NMR spectra of single crystals from two different batches. All experiments of this work are performed with the single crystal (I).

radii of lithium and copper are very similar, it required special efforts to satisfy the stoichiometry of this substance. Besides chemical methods described in Ref. 14, lithium unsoundness was controlled additionally with the NMR study of  $^7\text{Li}$  nuclei. Detailed NMR experiments in single crystalline  $\text{LiCuVO}_4$  in the paramagnetic phase are presented in Ref. 15. Figure 3 shows the NMR spectra obtained from two single crystals with different qualities, which are denoted as (I) and (II). The spectrum of the single crystal (II) consists of several lines which are due to defects, as it is described in Ref. 15. In the present work, all experiments are performed with the single crystal (I) which exhibits a single  $^7\text{Li}$  spectral line, demonstrating a unique lithium site. This single crystal (I) was selected from the same batch as the single crystals used in Ref. 2 and 3. The magnetic susceptibility was measured in the temperature range  $1.7 < T < 400$  K with a superconducting quantum interference device magnetometer MPMS5 of Quantum Design. The error of the magnetic susceptibility data is within the symbol size in Fig. 4. The AFMR experiments were performed with a transmission-type spectrometer using resonators in the frequency range

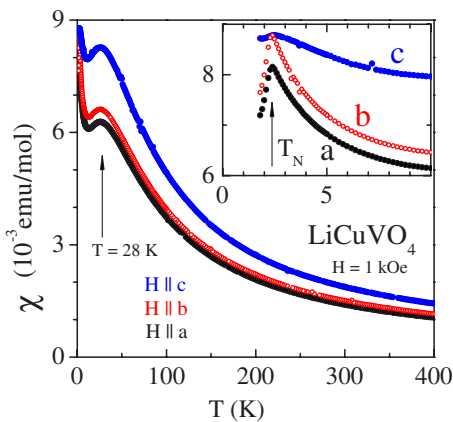


FIG. 4. (Color) Temperature dependences of the molar susceptibility  $\chi(T)$  of  $\text{LiCuVO}_4$ . The applied magnetic field of  $H=1$  kOe was directed along the principal axes **a**, **b**, and **c** of the single crystal. Inset: Magnification of the low-temperature range for  $T < 10$  K.

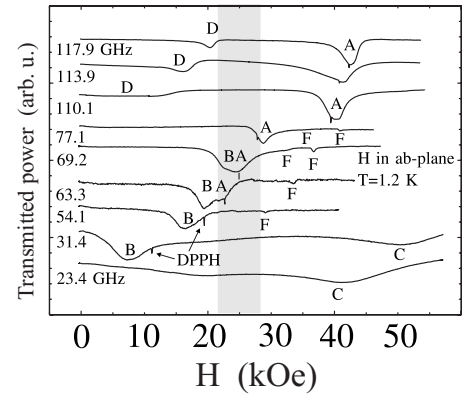


FIG. 5. Transmitted microwave power vs applied magnetic field  $H$  ( $\mathbf{H} \parallel \mathbf{ab}$  plane at 1.2 K). The signal of the reference compound diphenyl-picryl-hydrazyl (DPPH) is marked. For the denotations with capital letters A, ..., F, see text.

$18 < \nu < 110$  GHz. At elevated frequencies  $65 < \nu < 250$  GHz, we employed the waveguide-line technique. The magnetic field of the superconducting solenoid was varied in the range  $0 < H < 90$  kOe. Temperatures were varied within the range  $1.2 < T < 30$  K with a precision better than 0.1 K. The NMR experiments were performed with a phase coherent, homemade spectrometer at radio frequencies within the range  $14.5 < \nu < 170$  MHz. We investigated the  $^7\text{Li}$  ( $I=3/2$ ,  $\gamma/2\pi=16.5466$  MHz/T) and  $^{51}\text{V}$  ( $I=7/2$ ,  $\gamma/2\pi=11.2133$  MHz/T) nuclei using spin-echo technique with a pulse sequence  $5 \mu\text{s} - \tau_D - 10 \mu\text{s}$ , where the time between pulses  $\tau_D$  was  $40 \mu\text{s}$ . The spectra were collected by sweeping the applied magnetic field within  $8 < H < 93$  kOe at constant frequencies. Low temperatures  $0.6 < T < 3.3$  K were achieved with a  $^3\text{He}/^4\text{He}$  dilution refrigerator of Oxford Instruments. The temperatures were stabilized with a precision better than 0.02 K.

### III. MAGNETIC SUSCEPTIBILITY

Figure 4 displays the temperature dependence of the molar susceptibility  $\chi(T)$  of  $\text{LiCuVO}_4$  with the applied magnetic field  $H$  directed along the principal axes of the single crystal. The molar susceptibility  $\chi(T)$  exhibits two characteristic maxima: the high-temperature maximum around  $T \approx 28$  K is usual for low-dimensional magnetic systems and it is associated with the appearance of magnetic correlations within the copper chains. The sharp low-temperature maximum (cf. the inset of Fig. 4) is associated with the transition into a 3D magnetically ordered phase at  $T_N=2.3$  K (Refs. 15 and 16). The behavior of  $\chi(T)$  with respect to  $\mathbf{H} \parallel \mathbf{a}$  and  $\mathbf{H} \parallel \mathbf{b}$  is almost the same, but it essentially differs from  $\chi(T)$  for  $\mathbf{H} \parallel \mathbf{c}$ . In the paramagnetic phase and in the 3D ordered phase, the values of  $\chi(T)$  for  $\mathbf{H} \parallel \mathbf{c}$  are remarkably enhanced compared to  $\chi(T)$  for  $\mathbf{H}$  lying in the **ab** plane due to the anisotropy of the g tensor.<sup>16</sup>

### IV. ANTIFERROMAGNETIC RESONANCE

In Fig. 5, we show examples of traces of the transmitted

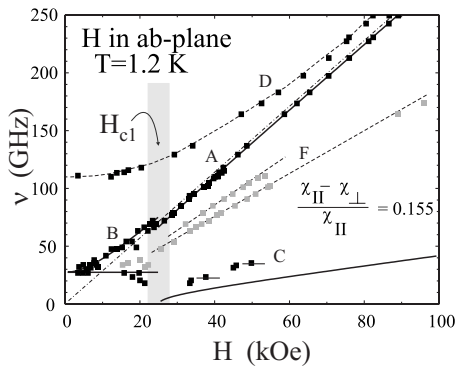


FIG. 6. AFMR spectra in the 3D ordered phase vs applied magnetic field  $H$  ( $\mathbf{H} \parallel \mathbf{ab}$  plane at 1.2 K). The capital letters mark the different branches of the spectra according to the denotations in Fig. 5.

microwave power, which are obtained by sweeping the applied magnetic field  $H$ . The orientation of  $\mathbf{H}$  was chosen to lie within the  $\mathbf{ab}$  plane. All traces were recorded at the temperature of  $T=1.2$  K, which is nearly two times less than  $T_N$ . The capital letters A, ..., D, and F denote absorption lines. Four absorption lines A, B, C, and D revealed intense signals, whereas the absorption line F is characterized by a narrow width and a tiny intensity. It turned out that the rotation of the applied magnetic field  $\mathbf{H}$  within the  $\mathbf{ab}$  plane does not change the position of the absorption lines. The resonance positions of these absorption lines A, ..., D, and F are plotted in Fig. 6 as a function of the magnetic field  $H$ . The resonance positions of the narrow line with a small intensity, which is marked with the letter F (the gray squares in Fig. 6), most probably have to be attributed to an electron paramagnetic resonance (EPR) of impurities in the sample. This assumption is corroborated by the observation of a decreasing intensity toward higher temperatures, but temperature independent resonance positions of these lines F. Therefore, the absorption lines F will not be discussed in our paper.

Within the field region  $22 \leq H \leq 28$  kOe, which is marked in light gray in Figs. 5 and 6, a peculiarity in the AFMR spectra was observed: toward lower fields  $H$ , branch A transforms into branch B exhibiting a coexistence of both absorption lines. The absorption line A appears at slightly higher fields and the absorption line B at slightly lower fields with respect to the resonance of the reference compound diphenyl-picryl-hydrazyl (DPPH) ( $g=2$ ), respectively (cf. Fig. 5). We associate this peculiarity for applied magnetic fields around 25 kOe with a phase transition, most probably of the spin-flop type at  $H_{c1} \approx 25$  kOe. For the orientation of the applied magnetic field  $\mathbf{H} \parallel \mathbf{c}$ , two branches A and D of the AFMR spectra were observed, as shown in Fig. 7. The dashed-dotted lines in Figs. 6 and 7 show the branches of EPR spectra, which were measured at 4.2 K. The values of the  $g$  factors at 4.2 K are in good agreement with the values reported in Ref. 16. The solid lines in Figs. 6 and 7 show the AFMR spectra which were deduced from a phenomenological theory for model systems as explained later in Sec. VII. The dashed lines in Figs. 6 and 7 are drawn for simplicity of perception.

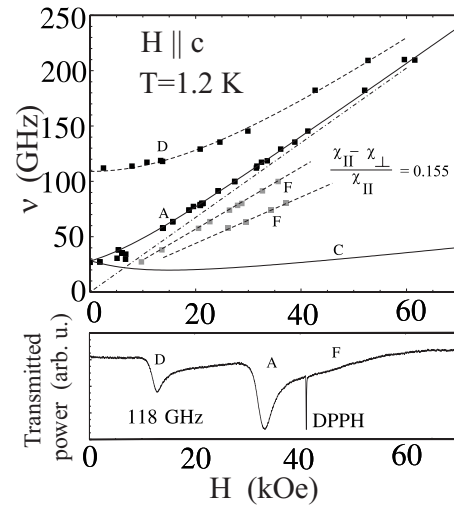


FIG. 7. Upper panel: AFMR spectra in the 3D ordered phase vs applied magnetic field  $H$  ( $\mathbf{H} \parallel \mathbf{c}$  at 1.2 K). The capital letters A, D, and F mark different branches of the spectra (see text). Lower panel: one example of the trace of the transmitted microwave power vs applied magnetic field  $H$  at 118 GHz ( $\mathbf{H} \parallel \mathbf{c}$  at 1.2 K). The signal of the reference compound DPPH is marked.

Figure 8 shows the angular dependence of the resonance field of the A branch on the angle  $\phi$  at the temperature of 1.2 K, where  $\phi$  is the angle between the direction of the applied magnetic field  $\mathbf{H}$  and the  $\mathbf{c}$  axis. The field  $\mathbf{H}$  is applied within the  $\mathbf{ac}$  plane. The open squares mark the values of EPR fields, measured in the paramagnetic phase at  $T=4.2$  K for  $\mathbf{H} \parallel \mathbf{a}$  and  $\mathbf{H} \parallel \mathbf{c}$ , respectively. At 78.5 GHz (upper

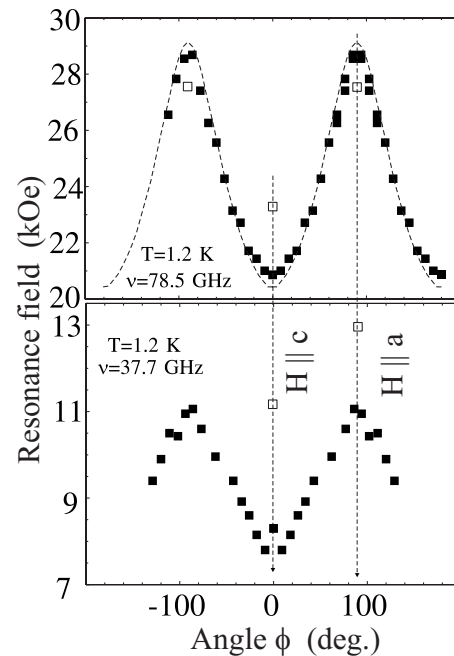


FIG. 8. Resonance field of the A branch vs  $\phi = \angle(\mathbf{H}, \mathbf{c})$  at  $T=1.2$  K. The field  $\mathbf{H}$  is applied within the  $\mathbf{ac}$  plane. The open squares mark the values of EPR fields measured in the paramagnetic phase ( $T=4.2$  K) for  $\mathbf{H} \parallel \mathbf{a}$  and  $\mathbf{H} \parallel \mathbf{c}$ , respectively. Upper panel:  $\nu=78.5$  GHz; lower panel:  $\nu=37.7$  GHz.

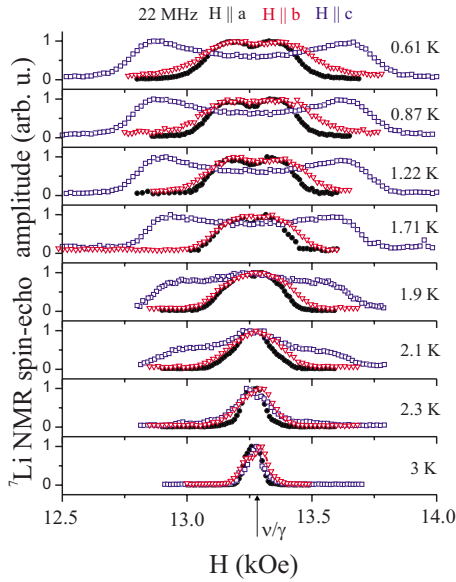


FIG. 9. (Color) Temperature dependence of  ${}^7\text{Li}$  NMR spectra at 22 MHz. The applied magnetic field  $\mathbf{H}$  was oriented along all crystallographic axes  $\mathbf{a}$ ,  $\mathbf{b}$ , and  $\mathbf{c}$ .

panel), the resonance field for the A branch occurs at a field value which is smaller than the field of the EPR signal when the field  $\mathbf{H}$  is applied along the  $\mathbf{c}$  axis ( $\mathbf{H}\parallel\mathbf{c}$ ). In case of the orientation  $\mathbf{H}\parallel\mathbf{a}$ , the resonance field for the A branch slightly exceeds the field of the EPR signal. The lower panel of Fig. 8 displays the situation at a frequency of 37.7 GHz. Here, the resonances according to this frequency appear at fields less than the transition field  $H_{c1} \approx 25$  kOe. In this case, the resonance fields for all angles  $\phi$  are less than the EPR fields. Note that the angular dependences of the resonance fields are predominantly defined by the angular dependence of the  $g$  factor.

## V. NUCLEAR MAGNETIC RESONANCE

Figures 9 and 10 show  ${}^7\text{Li}$  NMR spectra for different temperatures obtained at the frequencies of  $\nu=22$  and 50 MHz, respectively. The magnetic field  $H$  was applied along all crystallographic axes ( $\mathbf{H}\parallel\mathbf{a}$ ,  $\mathbf{H}\parallel\mathbf{b}$ , and  $\mathbf{H}\parallel\mathbf{c}$ ). These frequencies correspond to applied magnetic fields  $H$  which are lower than  $H_{c1} \approx 25$  kOe in the case of 22 MHz and higher than  $H_{c1}$  in the case of 50 MHz. For temperatures within the paramagnetic phase ( $T \geq 3$  K), the spectra for both frequencies are almost unshifted with respect to the reference field  $H_{\text{ref}} = \nu/\gamma$ , which is indicated by an arrow in Figs. 9 and 10. For decreasing temperatures toward  $T_N$ , the spectra start to broaden. For temperatures lower than  $T_N$ , the spectra change to a plateaulike shape with some increase of the intensity at their borders. Such shape of NMR spectra is characteristic for a spiral structure of the ordered electron moments, in which the magnetic ions induce different effective magnetic fields at the probing NMR nuclei, where the nuclei occupy crystallographically equivalent sites. From the fact of the temperature independent NMR line shape for temperatures  $0.6 < T < 1.2$  K, we conclude that the AFMR experi-

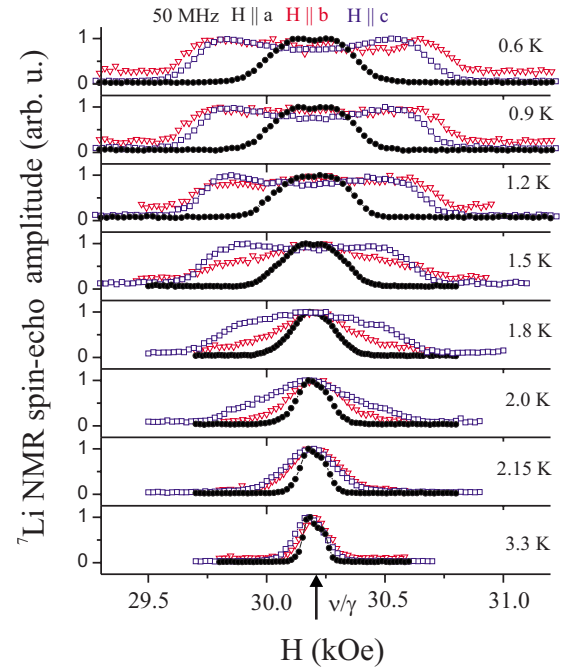


FIG. 10. (Color) Temperature dependence of  ${}^7\text{Li}$  NMR spectra at 50 MHz. The applied magnetic field  $\mathbf{H}$  was oriented along all crystallographic axes  $\mathbf{a}$ ,  $\mathbf{b}$ , and  $\mathbf{c}$ .

ments at 1.2 K were performed with nearly saturated magnetic  $\text{Cu}^{2+}$  moments.

At 22 MHz for applied fields  $H < H_{c1}$  (Fig. 9), the NMR spectrum at 0.6 K by application of the magnetic field along  $\mathbf{c}$  was approximately three times broader than the spectra observed by orientation of the field along  $\mathbf{a}$  and  $\mathbf{b}$ . We also measured at the frequency of 14.5 MHz (corresponding to an applied magnetic field around 8.8 kOe, not shown), and it turned out that the line shape at 0.6 K for  $\mathbf{H}\parallel\mathbf{b}$  is not changed compared to the spectrum obtained at 22 MHz (cf. uppermost frame of Fig. 9). At 50 MHz for applied fields exceeding  $H_{c1}$  (Fig. 10), the broad characteristic NMR spectra shape was observed for orientations of the magnetic field  $\mathbf{H}$  parallel to  $\mathbf{b}$  and  $\mathbf{c}$ . For the orientation  $\mathbf{H}\parallel\mathbf{a}$ , the NMR spectrum remains to be about three times narrower.

Figures 11 and 12 give the frequency and/or field dependence of  ${}^7\text{Li}$  NMR spectra in the paramagnetic phase at  $T = 3.3$  K and in the 3D magnetically ordered phase at  $T = 0.6$  K, respectively. In the paramagnetic phase at  $T = 3.3$  K (cf. Fig. 11), we observed one single unsplit spectral line for all frequencies and field orientations and a minor line shift with respect to the diamagnetic reference field  $H_{\text{ref}} = \nu/\gamma$ , which is indicated by an arrow in Fig. 11. For the field orientation  $\mathbf{H}\parallel\mathbf{a}$ , there is no frequency and/or field dependence of the  ${}^7\text{Li}$  NMR linewidth, whereas for  $\mathbf{H}\parallel\mathbf{b}$  and  $\mathbf{H}\parallel\mathbf{c}$  an appreciable increase of the  ${}^7\text{Li}$  NMR linewidth became apparent toward higher frequencies and/or fields as clearly seen in the uppermost frame of Fig. 11. In the 3D magnetically ordered phase at  $T = 0.6$  K (cf. Fig. 12), the linewidth of the characteristic spectra shape for  $\mathbf{H}\parallel\mathbf{c}$  turned out to be frequency and/or field independent up to the frequency of 100 MHz and/or field of 60.5 kOe, respectively. However,

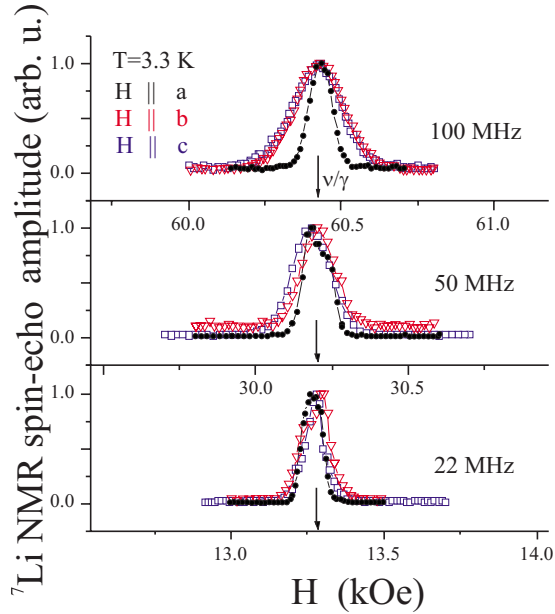


FIG. 11. (Color) Frequency dependence of  ${}^7\text{Li}$  NMR spectra in the paramagnetic phase at 3.3 K. The applied magnetic field  $\mathbf{H}$  was oriented along all crystallographic axes  $\mathbf{a}$ ,  $\mathbf{b}$ , and  $\mathbf{c}$ .

the line intensity of the central part of these spectra increases with increasing frequency and/or field. At 100 MHz and 60.5 kOe, a plateau-like shape evolved from the double-horn shape at 22 MHz and 13.25 kOe. As the frequency and/or

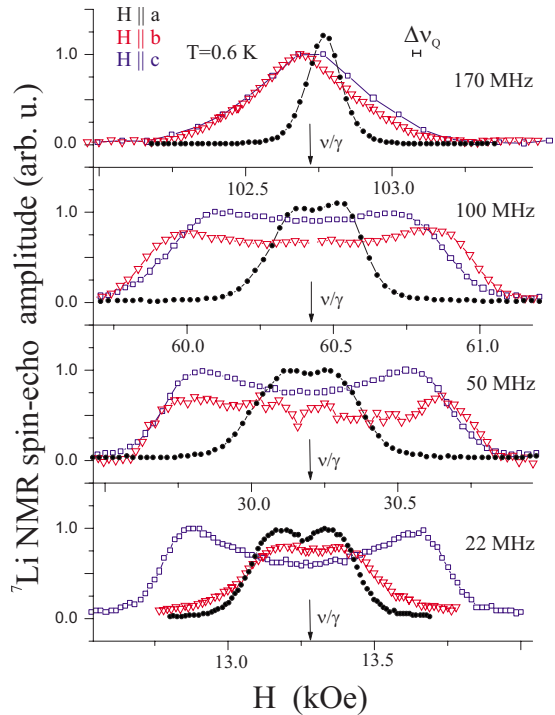


FIG. 12. (Color) Frequency dependence of  ${}^7\text{Li}$  NMR spectra in the 3D magnetically ordered phase at 0.6 K. The applied magnetic field  $\mathbf{H}$  was oriented along all crystallographic axes  $\mathbf{a}$ ,  $\mathbf{b}$ , and  $\mathbf{c}$ . The bar  $\Delta\nu_Q$  indicates the quadrupole contribution to the NMR line-width in the paramagnetic phase taken from Refs. 13 and 15.

field is further increased to 170 MHz and 102.75 kOe, the shape of the  ${}^7\text{Li}$  NMR spectra changes to one single unsplit spectral line (uppermost frame of Fig. 12). As high-field magnetization measurements revealed a spin reorientation taking place at an applied magnetic field of  $H_{c2} \approx 75$  kOe (Ref. 17), we interpolate from our data in Fig. 12 that the change to one single unsplit spectral line takes place at  $H_{c2} \approx 75$  kOe. The observed changes of the NMR line shape in Figs. 9–12, when the sample enters the magnetically ordered phase below  $T_N$ , are not blurred due to demagnetization effects of the sample shape. Demagnetization effects due to the sample shape are expected to be the same in the paramagnetic as in the ordered phase, because the magnetization around the Néel temperature  $T_N$  does not change drastically (cf. the inset in Fig. 4). Quantitatively, the upper bound of a broadening contribution due to demagnetization fields  $H = 4\pi M$  for  $\text{LiCuVO}_4$  is around 12 Oe at an applied magnetic field of 10 kOe. Therefore, our spectra measurements at 100 MHz and 60.5 kOe are expected to be broadened by demagnetization effects, which should be detectable in the paramagnetic phase only.

Figure 13 shows the orientation dependence of  ${}^{51}\text{V}$  NMR spectra in the 3D magnetically ordered phase at  $T=0.6$  K for  $\nu=100$  MHz. The intense narrow lines around 88.4 kOe are due to the  ${}^{63}\text{Cu}$  NMR signal from the copper wire of the resonant circuit. For all three crystallographic axes  $\mathbf{a}$ ,  $\mathbf{b}$ , and  $\mathbf{c}$ , the line splitting of the  ${}^{51}\text{V}$  NMR spectra amounts to five times the splitting of the  ${}^7\text{Li}$  NMR spectra. The characteristic NMR line shape of  ${}^{51}\text{V}$  for  $\mathbf{H}\parallel\mathbf{c}$  has also been observed in a recent NMR study at 120 kOe (Ref. 18). Due to a much stronger hyperfine coupling of the  ${}^{51}\text{V}$  nuclei,<sup>15</sup> the effective magnetic fields induced by the  $\text{Cu}^{2+}$  moments are strongly enhanced compared to the effective local fields induced at the  ${}^7\text{Li}$  nuclei. We also tried to detect  ${}^{51}\text{V}$  NMR spin-echo signals in the low-field range for  $H < H_{c1}$ , but for all three crystallographic axes  $\mathbf{a}$ ,  $\mathbf{b}$ , and  $\mathbf{c}$ , our attempts were unsuccessful. We attribute the lack of a vanadium signal to very short spin-spin relaxation times in this field range.

## VI. DISCUSSION OF NUCLEAR MAGNETIC RESONANCE EXPERIMENTS

The magnetic structure of  $\text{LiCuVO}_4$  is defined by strongly bonded chains of magnetic  $\text{Cu}^{2+}$  ions, directed along the crystallographic  $\mathbf{b}$  axis. The intra- and interchain exchange integrals are defined in Ref. 3: the intrachain exchange integrals  $J_1$  and  $J_2$  between nearest and next-nearest moments of copper ions in the chain are  $-1.6$  and  $5.6$  meV, respectively (cf. Fig. 1). The interchain exchange integrals  $J_3$ ,  $J_4$ ,  $J_5$ , and  $J_6$  between the chains given in Fig. 2 amount to  $0.01$ ,  $-0.37$ ,  $-0.014$ , and  $0.08$  meV, respectively.

The interchain interactions between the chains along the direction of the  $\mathbf{a}$  axis are defined by the exchange integrals  $J_3$  and  $J_4$  yielding a co-ordered arrangement of magnetic moments of neighboring copper ions in this direction. This interaction is much stronger than the interactions along the  $\mathbf{ac}$  diagonal ( $J_5$  and  $J_6$  in Fig. 2), which define the interchain interaction of magnetic moments in neighboring  $\mathbf{ab}$  planes. The simple evaluation of the exchange interactions with

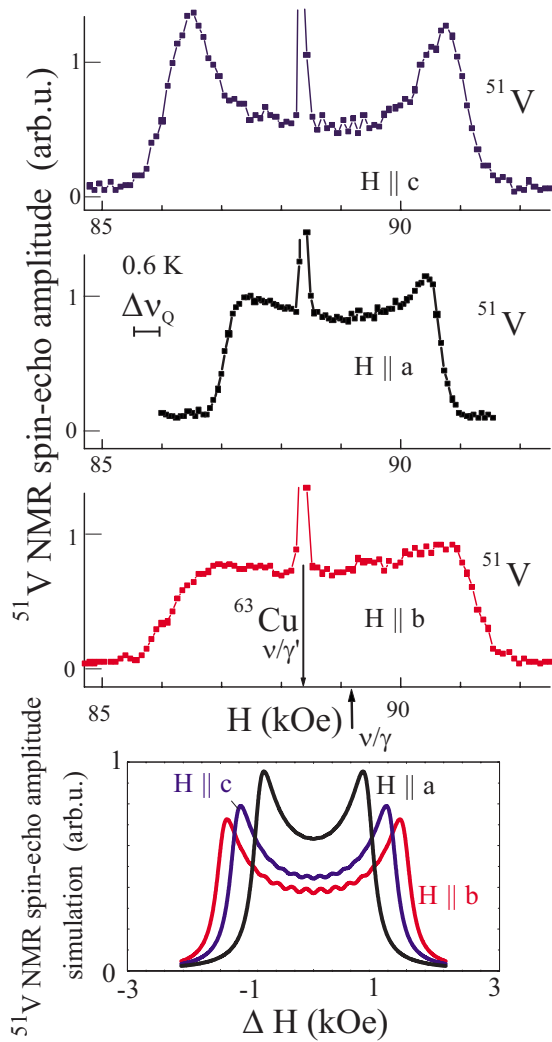


FIG. 13. (Color) Upper panel: orientation dependence of  $^{51}\text{V}$  NMR spectra in the 3D magnetically ordered phase at 0.6 K and 100 MHz. The applied magnetic field  $\mathbf{H}$  was oriented along all crystallographic axes  $\mathbf{a}$ ,  $\mathbf{b}$ , and  $\mathbf{c}$ . The bar  $\Delta\nu_Q$  indicates the quadrupole contribution to the NMR linewidth in the paramagnetic phase taken from Refs. 15 and 18. Lower panel: computed NMR spectra.

these values of exchange integrals gives the following hierarchy of energy of interactions recomputed on one magnetic ion: the ferromagnetic interaction between the chains within the  $\mathbf{ab}$  planes is about 1 order of magnitude less than the intrachain interactions and around ten times larger than the antiferromagnetic interaction between neighboring  $\mathbf{ab}$  planes. The magnetic moments of  $\text{Cu}^{2+}$  ions in the neighboring  $\mathbf{ab}$  planes are oriented antiparallel.<sup>2</sup>

In the present paper, we study NMR on  $^7\text{Li}$  and  $^{51}\text{V}$  nuclei. In Fig. 2, the positions of one  $\text{Li}^+$  ion and one  $\text{V}^{5+}$  ion are shown exemplarily, and it turns out that the lattice positions of these ions are essentially different: the position of the  $\text{Li}^+$  ions contains the operation of inversion, but the position of  $\text{V}^{5+}$  does not. The  $^7\text{Li}$  nuclei reside on positions between neighboring  $\mathbf{ab}$  planes. Every lithium ion has four nearest copper ions, which are equally distanced from it. Each vanadium ion resides between six neighboring copper

ions, where four of them belong to one  $\mathbf{ab}$  plane and two, more distant, to another  $\mathbf{ab}$  plane. We want to point out that the local symmetry at the probing nuclear sites of  $^7\text{Li}$  as well as  $^{51}\text{V}$  yields an electric field gradient which interacts with the nuclear quadrupole moments of  $^7\text{Li}$  (Refs. 13 and 15) and  $^{51}\text{V}$  (Refs. 15 and 18), respectively. This interaction contributes to the linewidth  $\Delta_{\text{NMR}}$  of the NMR spectra in the paramagnetic phase as it is indicated by the bars  $\Delta\nu_Q$  in Figs. 12 and 13. The values of  $\Delta\nu_Q$  are taken from Refs. 13, 15, and 18. Here, the linewidth in the magnetically ordered phase is about 33 times  $\Delta_{\text{NMR}}$  in case of  $^7\text{Li}$  and about ten times  $\Delta_{\text{NMR}}$  in the case of  $^{51}\text{V}$ , respectively. Such a tremendous increase of the linewidth cannot be attributed to the electric quadrupole interaction, because it would require an appreciable change of the crystallographic structure which is excluded from neutron scattering in Ref. 2. It is important to note that Gibson *et al.* report about a full refinement of the nuclear structure at *zero* applied magnetic field only, which was obtained by elastic neutron-diffraction measurements down to temperatures  $T \approx 0.15$  K. Only a slight temperature-induced lattice contraction had been observed.<sup>2</sup> Further elastic neutron-diffraction measurements in applied magnetic fields are needed in order to exclude field-induced distortions of the crystallographic structure which might affect the NMR line shapes.

The effective local fields at the probing nuclei of the non-magnetic lithium and vanadium ions are composed of the long-range dipole fields of surrounding magnetic moments and of the so-called contact hyperfine fields due to the nearest magnetic ions. The contact fields are expected to be proportional to the spin values of the neighboring copper ions. The contact fields at the  $^7\text{Li}$  nuclei must be self-compensated in the case of the antiparallel magnetic ordering of the nearest magnetic moments of the neighboring  $\mathbf{ab}$  planes. At the  $^{51}\text{V}$  nuclei, the contact fields will be predominantly given by the spins of the four nearest magnetic ions of the nearest neighboring  $\mathbf{ab}$  plane (cf. Fig. 2). The value of the long-range dipole field was computed for the positions of  $^7\text{Li}$  and  $^{51}\text{V}$  nuclei by assumption of the spiral-magnetic structure proposed in Ref. 2. For this structure, the magnetic moments of the copper ions can be calculated as follows:

$$\boldsymbol{\mu} = \mu_{\text{Cu}} \mathbf{I}_1 (-1)^{2z/c} \cos(k_{ic} \cdot \mathbf{y}) + \mu_{\text{Cu}} \mathbf{I}_2 (-1)^{2z/c} \sin(k_{ic} \cdot \mathbf{y}), \quad (1)$$

where the coordinates  $x, y$ , and  $z$  are given in the basis of the crystal axes  $\mathbf{a}$ ,  $\mathbf{b}$ , and  $\mathbf{c}$ . The vectors  $\mathbf{I}_1$  and  $\mathbf{I}_2$  are orthogonal unit vectors within the  $\mathbf{ab}$  plane. Consequently, the vector of the exchange structure  $\mathbf{n} = \mathbf{I}_1 \times \mathbf{I}_2$  is parallel to the  $\mathbf{c}$  axis. The values of the lattice parameters  $a$ ,  $b$ , and  $c$  and the coordinates of lithium and vanadium ions were taken from Ref. 19. For the value of the ordered magnetic moment  $\mu_{\text{Cu}}$  of the copper ions, we took  $0.31 \mu_B$  as it was obtained in Ref. 2.

$H < H_{c1}$ . The dipole field at the  $^7\text{Li}$  nuclei depends on their positions within the incommensurate spiral-magnetic structure. In the upper panel of Fig. 14, the projections of dipole fields on the  $\mathbf{a}$ ,  $\mathbf{b}$ , and  $\mathbf{c}$  axes are plotted as a function of the phase of the spiral-magnetic structure. From these fields, it is simple to simulate the expected NMR spectra for

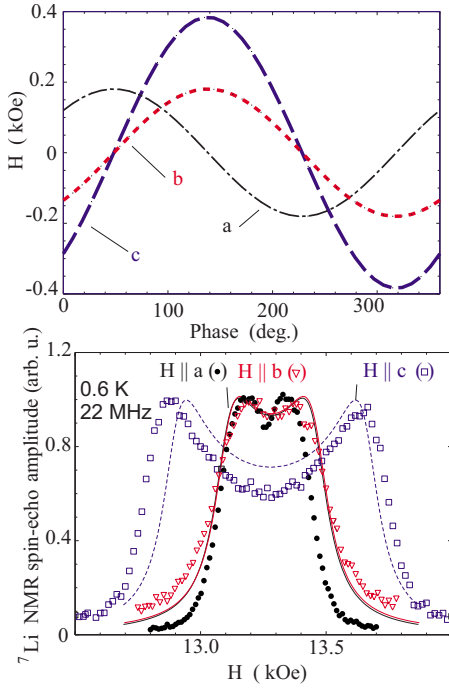


FIG. 14. (Color) Upper panel: computed projections of dipole fields along the **a**, **b**, and **c** axes as a function of the phase of the spiral-magnetic structure  $\mathbf{n}\parallel\mathbf{c}$  suggested in Ref. 2. Lower panel: experimental  ${}^7\text{Li}$  NMR spectra measured at  $T=0.6$  K for  $H < H_{c1}$  (symbols) and computed NMR spectra (dashed and solid lines).

all three directions of the applied magnetic field  $H$  with respect to the crystallographic axes. The lower panel of Fig. 14 shows computed spectra (dashed and solid lines) and experimental data (symbols) for the frequency of 22 MHz. This computation was performed with a Lorentzian shape of the NMR spectrum, which is produced by the group of  ${}^7\text{Li}$  nuclei experiencing the same value of the effective local magnetic field. The linewidth of this Lorentzian-shaped spectrum was assumed to be equal to 75 Oe. This value of the linewidth is consistent with the linewidth in the paramagnetic phase of the low-field range (Fig. 9). The computed NMR spectra are in a very good agreement with the experimental spectra. This means that the effective local fields at the  ${}^7\text{Li}$  nuclei are predominantly defined by long-range dipole fields, and we should be able to specify the magnetic structures of  $\text{LiCuVO}_4$  for elevated applied magnetic fields  $H > H_{c1}$ .

$H_{c1} < H < H_{c2}$ . The most natural magnetic transition taking place with increasing applied magnetic fields  $H$  is the spin-flop transition, i.e., the rotation of the plane of the spiral spin structure perpendicular to the direction of the applied magnetic field  $H$ . Therefore, for  $\mathbf{H}\parallel\mathbf{c}$ , there will be no spin reorientation expected. Indeed, the experiment exhibits nearly the same pattern of the NMR spectra for  $\mathbf{H}\parallel\mathbf{c}$  at all frequencies of 22, 50, and 100 MHz, corresponding to applied magnetic fields around  $H_{c1} \approx 25$  kOe (cf. Fig. 12). Applying a magnetic field  $H > H_{c1}$  parallel to the **a** and **b** axes may result in a rotation of the magnetic structure and the line shapes can concomitantly change. Figure 15 shows the results of the computation of the NMR spectra for these structures together with the experimental NMR spectra measured

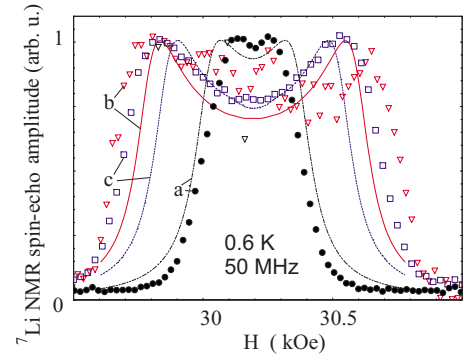


FIG. 15. (Color) Experimental  ${}^7\text{Li}$  NMR spectra measured at  $T=0.6$  K and  $H > H_{c1}$  (symbols) and computed NMR spectra (dashed and solid lines).

at the frequency of 50 MHz. The computation and experiment show that the spin reorientation drastically broadens the NMR spectra for  $\mathbf{H}\parallel\mathbf{b}$ , and nearly no change is observed for  $\mathbf{H}\parallel\mathbf{a}$ . This magnetic structure is maintained up to applied magnetic fields  $H \approx 60.5$  kOe  $< H_{c2}$ , as it is seen from the NMR spectra pattern at 100 MHz and 60.5 kOe in Fig. 12. Thus, for  $H_{c1} < H < H_{c2}$ , the magnetic structure exhibits the spiral plane perpendicular to the applied magnetic field  $\mathbf{H}\parallel\mathbf{n}$  [cf. Eq. (1)] for  $\mathbf{H}\parallel\mathbf{b}$  and  $\mathbf{H}\parallel\mathbf{c}$ , respectively. The agreement of the experimental and computed spectra was only possible to obtain in the case of an antiferromagnetic alternation of the magnetic moments of the neighboring **ab** planes (cf. Fig. 2).

$H > H_{c2}$ . A more complicated situation occurs at high fields  $H > H_{c2}$ : the NMR spectra of  ${}^7\text{Li}$  nuclei in this field range consist of one single line for all field directions (cf. the uppermost panel in Fig. 12), indicating a second spin reorientation process to take place. For the high-field range  $H > H_{c2}$ , it was possible to measure NMR spectra of the  ${}^{51}\text{V}$  nuclei, too. To understand the nature of the effective local field at the  ${}^{51}\text{V}$  nuclei, we computed the long-range dipole field at the vanadium site for the paramagnetic phase. The computed dipole field is  $-0.44$  kOe/ $\mu_B$  for the direction of the applied field  $\mathbf{H}$  parallel to the **b** axis. However, the value of the hyperfine coupling constant  ${}^{51}A_{\parallel b} = 4.95$  kOe/ $\mu_B$  is about ten times larger as we obtained in Ref. 15. Thus, we can conclude that the main part of the effective local field at the  ${}^{51}\text{V}$  nuclei is defined by contact fields. The value of the effective contact field induced by copper ions at the vanadium nuclei can be evaluated as  $5.4[(\mu_{\text{Cu}1} + \mu_{\text{Cu}2} + \mu_{\text{Cu}3} + \mu_{\text{Cu}4})/4]$  kOe/ $\mu_B$ . Here, we take into account only the four nearest magnetic copper ions from the nearest neighboring **ab** plane (Fig. 2).

The characteristic broad NMR spectra of  ${}^{51}\text{V}$  nuclei (Fig. 13) in the 3D magnetically ordered phase for  $H > H_{c2}$  indicate a modulation of the projection of the  $\text{Cu}^{2+}$  moments on the direction of the applied field  $\mathbf{H}$ . A more simple way to describe this modulation is to suppose that at  $H_{c2}$  the spiral planar magnetic structure is oriented parallel to the applied field  $H$  (i.e.,  $\mathbf{n} \perp \mathbf{H}$ ). We computed the value of the effective local fields at the  ${}^{51}\text{V}$  nuclei using the same parameters  $k_{ic}$  and  $\mu_{\text{Cu}}$  of the spiral-magnetic structure at zero applied field

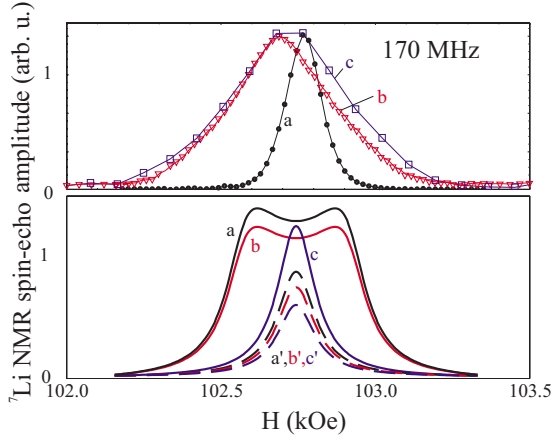


FIG. 16. (Color) Upper panel: experimental  ${}^7\text{Li}$  NMR spectra measured at  $T=0.6$  K and  $H>H_{c2}$ . The applied magnetic field  $\mathbf{H}$  was oriented along all crystallographic axes  $\mathbf{a}$ ,  $\mathbf{b}$ , and  $\mathbf{c}$ . Lower panel: computed NMR spectra for spiral- (solid lines,  $\mathbf{a}$ ,  $\mathbf{b}$ , and  $\mathbf{c}$ ) and spin-modulated (dashed lines,  $\mathbf{a}'$ ,  $\mathbf{b}'$ , and  $\mathbf{c}'$ ) structures, respectively.

$H=0$ . The computed NMR spectra with these parameters are shown in the lowest panel of Fig. 13. Again, this computation was performed with a Lorentzian shape of the NMR spectrum, which is produced by the group of  ${}^{51}\text{V}$  nuclei experiencing the same value of the effective local magnetic field. The linewidth of this Lorentzian-shaped spectrum was assumed to be equal to 150 Oe. Note that the computed NMR spectra fit better if the value of  $\mu_{\text{Cu}}$  is increased and/or the value of  $k_{ic}$  is decreased.

Changing again to the  ${}^7\text{Li}$  NMR spectra for  $H>H_{c2}$  (cf. upper panel in Fig. 16), the unsplit line shapes of the NMR spectra suggest the following magnetic structures which are deduced from computations of dipole fields for different planar spiral structures: For  $\mathbf{H}\parallel\mathbf{c}$ , the best fit is obtained for  $\mathbf{n}\parallel\mathbf{b}$ . For  $\mathbf{H}\parallel(\mathbf{a},\mathbf{b})$ , the plane of the spiral structure lies within the  $\mathbf{ab}$  plane (i.e.,  $\mathbf{n}\parallel\mathbf{c}$ ). In the lower panel of Fig. 16, the results of the computed NMR spectra are shown for these spiral structures. For field orientations parallel to the  $\mathbf{a}$  and  $\mathbf{b}$  axes, the computed spectra exhibit some splitting of the spectra shape contrary to the experiment. Due to this lack of any splitting of the experimental spectra for  $H>H_{c2}$ , we conclude that *not* the spiral, but a spin-modulated structure is realized; i.e., the spin projections perpendicular to the direction of the applied field  $H$  are disordered. The NMR spectra computed for this spin-modulated structure are shown in the same figure (dashed lines in the lower panel of Fig. 16). All spectra for this structure are unsplit. This computation was performed with a linewidth of 150 Oe of the Lorentzian-shaped NMR spectrum, which is produced by the group of  ${}^7\text{Li}$  nuclei experiencing the same value of the effective local magnetic field. In order to achieve a better fit for field directions  $\mathbf{H}\parallel(\mathbf{b},\mathbf{c})$ , this value of the linewidth has to be increased by a factor of 2.8. At first glance, this increase seems to be arbitrary, but on closer inspection of the experimental spectra in the paramagnetic phase (uppermost panel of Fig. 11), the spectral linewidths for field directions  $\mathbf{H}\parallel(\mathbf{b},\mathbf{c})$  are also significantly increased compared to  $\mathbf{H}\parallel\mathbf{a}$ .

## VII. DISCUSSION OF ANTIFERROMAGNETIC RESONANCE EXPERIMENTS

For low applied magnetic fields  $H<H_{c1}$ , the authors of Ref. 2 propose the planar spiral structure for the magnetic structure of  $\text{LiCuVO}_4$  in the 3D magnetically ordered phase. This structure was found to be defined by strong exchange interactions within the magnetic chains.<sup>3</sup> Our results of the NMR and susceptibility  $\chi$  investigations can be explained on the same footing. The results of EPR (Ref. 16) and AFMR (this work) hint toward an uniaxial character of the crystal anisotropy in  $\text{LiCuVO}_4$ . These observations motivate us to discuss the low-field AFMR data in the assumptions of an exchange-rigid planar uniaxial magnetic structure with an uniaxial crystal anisotropy, which is directed along the  $\mathbf{c}$  axis. Thus, we will suppose that the susceptibility of the exchange structure will be defined by two values  $\chi_{\parallel}$  and  $\chi_{\perp}$ , i.e., along and perpendicular to the vector of the exchange structure  $\mathbf{n}$  [cf. Eq. (1)], respectively. The anisotropy energy within this model can be written in a form  $\beta n_z^2/2$  ( $\beta<0$ ). The NMR and AFMR data reveal a magnetic transition at  $H_{c1}$ , if the magnetic field  $H$  is applied parallel to the  $\mathbf{ab}$  plane. This implies that  $\chi_{\parallel}$  is larger than  $\chi_{\perp}$ , and the transition field can be described as  $H_{c1}^2=\beta/(\chi_{\perp}-\chi_{\parallel})$ .

In Ref. 20, the low-frequency branches of the AFMR spectra for noncollinear coplanar structures with an uniaxial anisotropy were obtained in the framework of a phenomenological theory according to Ref. 21. The spectra of acoustic modes consist of three branches, which correspond to three rotational degrees of freedom. In the case of an uniaxial exchange structure, one branch out of these three branches must be zero ( $\nu=0$ ), which is attributed to the rotational degree of freedom of the exchange structure around the  $\mathbf{n}$  axis. The frequencies of the two other branches can be obtained from the following square equation:

$$\begin{aligned} (\nu/\gamma)^4 - (\nu/\gamma)^2\{H^2 + \eta^2 H^2 \cos^2(\theta - \phi) + \eta H_{c1}^2(3 \cos^2 \theta - 1)\} \\ + \eta\{-H_{c1}^2 \cos^2 \theta - H^2 \cos^2(\theta - \phi)\} - \eta H_{c1}^2 \cos 2\theta \\ - \eta H^2 \cos^2(\theta - \phi) - H^2 \sin^2(\theta - \phi) = 0, \end{aligned} \quad (2)$$

where  $\gamma=g\mu_B/2\pi\hbar$ ,  $\eta=(\chi_{\parallel}-\chi_{\perp})/\chi_{\perp}$ , and  $\phi=\angle(\mathbf{H},\mathbf{c})$  is the angle between the crystallographic  $\mathbf{c}$  axis and the direction of the applied magnetic field  $\mathbf{H}$ . The angle  $\theta=\angle(\mathbf{n},\mathbf{c})$  is defined by

$$\tan(2\theta) = \frac{H^2 \sin 2\phi}{H^2 \cos(2\phi) + H_{c1}^2}.$$

If the applied magnetic field is directed along the  $\mathbf{c}$  axis ( $\mathbf{H}\parallel\mathbf{c}$ ), both angles are zero ( $\theta=0$ ,  $\phi=0$ ), whereas for  $\mathbf{H}\perp\mathbf{c}$ ,  $H<H_{c1}$ ,

$$\theta=0, \quad \phi=\pi/2,$$

and for  $\mathbf{H}\perp\mathbf{c}$ ,  $H>H_{c1}$ ,

$$\theta=\pi/2, \quad \phi=\pi/2.$$

At zero applied field  $H=0$ , the frequency of both oscillations must be  $\nu_{1,2}=\gamma H_{c1}\sqrt{\eta}$ . Taking the frequency of  $27\pm 2$  GHz of the AFMR at zero applied field and the field  $H_{c1}$  of the spin-flop transition to be  $H_{c1}=25\pm 3$  kOe, we obtain the pa-

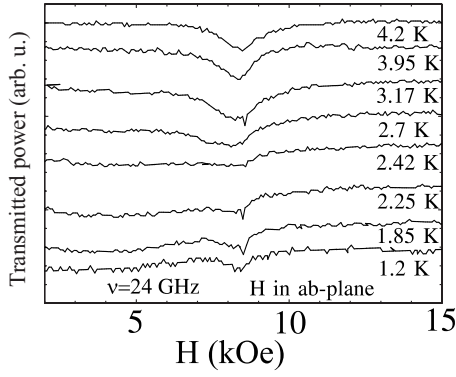


FIG. 17. Transmitted microwave power vs applied magnetic field  $H$  for different temperatures at 24 GHz. The field  $\mathbf{H}$  is applied within the  $\mathbf{ab}$  plane.

parameter of the anisotropy of the exchange susceptibility  $\eta = 0.155 \pm 0.05$  and the value of the anisotropy constant  $\beta \approx -0.01$  K, recomputed on one copper ion. The results of the computation of the A, B, and C branches of the AFMR spectra for  $\eta = 0.155$  are shown as solid lines in Figs. 6 and 7. The value of the anisotropy of the exchange parameter  $\eta$  is in satisfactory agreement with the value obtained from susceptibility measurements at low fields (Fig. 4). Note that the theory of AFMR spectra discussed above is developed in an exchange approximation with isotropic  $\gamma$ . For the computed spectra shown in Figs. 6 and 7, we used the values of  $\gamma_{\parallel} = 3.25$  GHz/kOe and  $\gamma_{\perp} = 2.85$  GHz/kOe, which were measured in the paramagnetic phase. We can conclude that this model describes the AFMR spectra within the low-field range ( $H \ll H_{c2}$ ) very well.

On closer inspection of the experimental AFMR data in Figs. 6 and 7 for applied fields  $H \rightarrow 0$ , there are two branches which exhibit a frequency-axis intercept of  $\nu(H=0) \approx 25$  and  $\approx 108$  GHz, respectively. These two intercepts at 1.2 K deep in the 3D magnetically ordered phase identify two excitation gaps which turned out to have different temperature dependences: the low-frequency gap decreases with increasing temperatures and the corresponding branch becomes gapless at a temperature near  $T_N$ . In Fig. 17, traces of the transmitted microwave power are displayed as a function of the applied magnetic field  $H$  for different temperatures at  $\nu = 24$  GHz. Toward decreasing temperatures, the AFMR line starts to broaden at a temperature  $T \approx T_N$  and shifts toward lower fields. At 1.2 K, the broad line at zero field  $H=0$  shows that the probing frequency of 24 GHz is almost equal to the gap value at this temperature. Using Eq. (2), analogous spectra obtained at the probing frequency of  $\nu = 38$  GHz allow us to obtain the temperature dependence of the gap value, which is shown in the lower panel of Fig. 18. The high-frequency gap, which has to be attributed to the D branch, remains to be open till much higher temperatures than  $T_N$ . The upper panel of Fig. 18 shows traces of the transmitted microwave power as a function of the applied magnetic field  $H$  for different temperatures at  $\nu = 113$  GHz ( $\mathbf{H} \parallel \mathbf{a}$ ). The AFMR position of the D branch is well defined till  $T \approx 10$  K. The temperature dependence of this AFMR position is documented in the lower panel of Fig. 18, indicating the gap of the D branch at

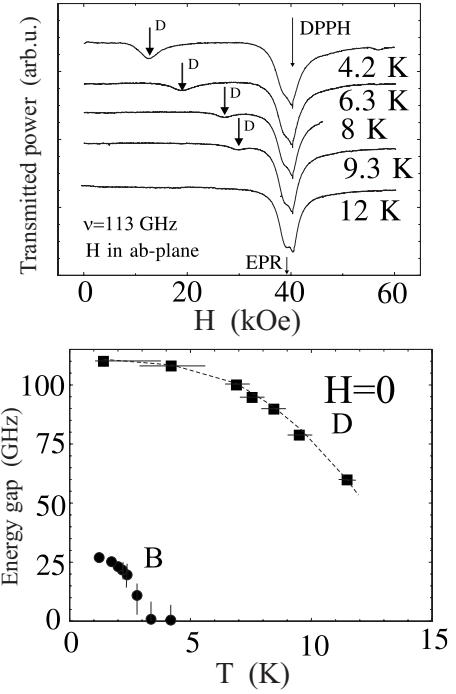


FIG. 18. Upper panel: transmitted microwave power vs applied magnetic field  $H$  for different temperatures at 113 GHz ( $\mathbf{H} \parallel \mathbf{a}$ ). Lower panel: temperature dependence of the AFMR positions of B and D branches at zero field  $H=0$ .

zero applied magnetic field. The continuous decrease of the AFMR frequency toward higher temperatures indicates the closing of the gap. From the extrapolation of this continuous decrease to zero frequency, we expect the D branch to be gapless at the temperature of  $T \approx 13$  K.

The magnetic phase  $H$ - $T$  diagram of  $\text{LiCuVO}_4$  is rich not only in field cut but also in temperature. It seems that the establishment of the 3D magnetic order appears through some intermediate phase transition. This we conclude from the fact that the AFMR branch D in Figs. 6 and 7 starts to be gapped at a temperature around 13 K much higher than  $T_N$  (Fig. 18). The fingerprint of this transition around  $T = 13$  K additionally has recently been detected in measurements of the temperature dependence of the heat capacity,<sup>22</sup> where a peak of  $C(T)$  centered at  $T = 12$  K has been reported.

## VIII. CONCLUSION

The NMR and AFMR results can be self-consistently described by the following phase diagram:

$$H < H_{c1}: \mathbf{n} \parallel \mathbf{c},$$

$$H_{c1} < H < H_{c2}: \mathbf{n} \parallel \mathbf{H},$$

$$H_{c2} < H: \mathbf{l}_1 \parallel \mathbf{H} \text{ and } \mathbf{l}_2 = 0,$$

where the magnetic structures are described in terms of Eq. (1). It is important to note that for  $H > H_{c2}$ , from our experiments, we can surely conclude only about the presence of a modulation of projections of copper moments along the di-

rection of the applied magnetic field  $H$  with an amplitude of  $\approx 0.4 \pm 0.1 \mu_B$ . The best fit of  $^7\text{Li}$  NMR spectra is obtained based on a spin-modulated structure, i.e., the spin components of the  $\text{Cu}^{2+}$  moment, which are oriented perpendicular to the direction of the applied magnetic field  $H$ , are disordered.

The low-field phases for  $H < H_{c2}$  observed in  $\text{LiCuVO}_4$  are natural from the point of view of the mean-field theory. The susceptibility of the exchange structure in the direction perpendicular to the  $\mathbf{a}$ ,  $\mathbf{b}$  plane is larger than the susceptibility within this plane. The competition of the Zeeman energy and the energy of the crystal-field anisotropy explains the low-field transition observed at  $H_{c1}$ . The second transition at the field  $H_{c2}$  is unusual. To explain this transition, we have to assume that with an increase of the applied magnetic field, the structure starts to be preferable which exhibits the spin modulation parallel to the direction of the applied magnetic field, rather than the structure with the spin plane being per-

pendicular to the field direction. Probably, it is necessary to take into account the thermal and quantum fluctuations in order to explain the situation. For example, for the planar spiral structure on the triangular lattice, it was found that some energy gain occurs for the orientation of the spin plane to be parallel to the direction of the applied magnetic field.<sup>23</sup>

#### ACKNOWLEDGMENTS

We are grateful to A. Pimenova and D. Vieweg for susceptibility measurements. We thank V. N. Glazkov, V. I. Marchenko, A. I. Smirnov, S. S. Sosin, G. B. Teitelbaum, and A. Loidl for useful discussions. This work is supported by the Grant No. 07-02-00725 and No. 06-02-16509 of the Russian Foundation for Basic Research, Russian President Program of Scientific Schools, contract BMBF via VDI/EKM 13N6917, and program of the German Research Society within the Sonderforschungsbereich 484 (Augsburg).

\*norbert.buettgen@physik.uni-augsburg.de

<sup>†</sup>Present address: Institut für Festkörperphysik, Technische Universität Wien, A-1040 Wien, Austria.

<sup>1</sup>G. Blasse, *J. Phys. Chem. Solids* **27**, 612 (1966).

<sup>2</sup>B. J. Gibson, R. K. Kremer, A. V. Prokofiev, W. Assmus, G. J. McIntyre, *Physica B* **350**, 253 (2004).

<sup>3</sup>M. Enderle, C. Mukherjee, B. Fåk, R. K. Kremer, J.-M. Broto, H. Rosner, S.-L. Drechsler, J. Richter, J. Malek, A. Prokofiev, W. Assmus, S. Pujol, J.-L. Raggazzoni, H. Rakoto, M. Rheinstädter, and H. M. Rønnow, *Europhys. Lett.* **70**, 237 (2005).

<sup>4</sup>R. Coldea, D. A. Tennant, A. M. Tselik, and Z. Tylczynski, *Phys. Rev. Lett.* **86**, 1335 (2001).

<sup>5</sup>T. Ono, H. Tanaka, H. Aruga Katori, F. Ishikawa, H. Mitamura, and T. Goto, *Phys. Rev. B* **67**, 104431 (2003); T. Ono, H. Tanaka, O. Kolomyiets, H. Mitamura, T. Goto, K. Nakajima, A. Oosawa, Y. Koike, K. Kakurai, J. Klenke, P. Smeibidle, and M. Meissner, *J. Phys.: Condens. Matter* **16**, S773 (2004).

<sup>6</sup>H. Katsura, N. Nagaosa, and A. V. Balatsky, *Phys. Rev. Lett.* **95**, 057205 (2005); M. Mostovoy, *ibid.* **96**, 067601 (2006).

<sup>7</sup>Y. Naito, K. Sato, Y. Yasui, Y. Kobayashi, Y. Kobayashi, and M. Sato, *J. Phys. Soc. Jpn.* **76**, 023708 (2007).

<sup>8</sup>A. N. Vasil'ev, *Pis'ma Zh. Eksp. Teor. Fiz.* **69**, 828 (1999) [*JETP Lett.* **69**, 876 (1999)].

<sup>9</sup>Y. Mizuno, T. Tohyama, S. Maekawa, T. Osafune, N. Motoyama, H. Eisaki, and S. Uchida, *Phys. Rev. B* **57**, 5326 (1997).

<sup>10</sup>S. R. White and I. Affleck, *Phys. Rev. B* **54**, 9862 (1996).

<sup>11</sup>R. Bursill, G. A. Gehring, D. J. J. Farnell, J. B. Parkinson, Tao Xiang, and Chen Zeng, *J. Phys.: Condens. Matter* **7**, 8605 (1995).

<sup>12</sup>A. V. Prokofiev, D. Wichert, and W. Aßmus, *J. Cryst. Growth*

**220**, 345 (2000).

<sup>13</sup>Ch. Kegler, N. Büttgen, H.-A. Krug von Nidda, A. Krimmel, L. Svistov, B. I. Kochelaev, A. Loidl, A. Prokofiev, and W. Assmus, *Eur. Phys. J. B* **22**, 321 (2001).

<sup>14</sup>A. V. Prokofiev, I. G. Vasilyeva, V. N. Ikorskii, V. V. Malakhov, I. P. Asanov, and W. Aßmus, *J. Solid State Chem.* **177**, 3131 (2004).

<sup>15</sup>C. Kegler, N. Büttgen, H.-A. Krug von Nidda, A. Loidl, R. Nath, A. V. Mahajan, A. V. Prokofiev, and W. Aßmus, *Phys. Rev. B* **73**, 104418 (2006).

<sup>16</sup>H.-A. Krug von Nidda, L. E. Svistov, M. V. Eremin, R. M. Eremina, A. Loidl, V. Kataev, A. Validov, A. Prokofiev, and W. Aßmus, *Phys. Rev. B* **65**, 134445 (2002).

<sup>17</sup>M. G. Banks, F. Heidrich-Meisner, A. Honecker, H. Rakoto, J.-M. Broto, and R. K. Kremer, *J. Phys.: Condens. Matter* **19**, 145227 (2007).

<sup>18</sup>R. Smith, A. P. Reyes, R. Ashey, T. Caldwell, A. Prokofiev, W. Aßmus, and G. Teitelbaum, *Physica B* **378-380**, 1060 (2006).

<sup>19</sup>R. Kanno, Y. Kawamoto, Y. Takeda, M. Hasegawa, O. Yamamoto, and N. Kinomura, *J. Solid State Chem.* **96**, 397 (1992).

<sup>20</sup>I. A. Zaliznyak, V. I. Marchenko, S. V. Petrov, L. A. Prozorova, and A. V. Chubukov, *Pis'ma Zh. Eksp. Teor. Fiz.* **47**, 172 (1988) [*JETP Lett.* **47**, 211 (1988)].

<sup>21</sup>A. F. Andreev and V. I. Marchenko, *Usp. Fiziol. Nauk* **130**, 39 (1980) [*Sov. Phys. Usp.* **23**, 21 (1980)].

<sup>22</sup>M. G. Banks, R. K. Kremer, A. Honecker, and F. Heidrich-Meisner, contribution to the Conference on Highly Frustrated Magnetism, 2006, Osaka, Japan (unpublished).

<sup>23</sup>A. V. Chubukov and D. I. Golosov, *J. Phys.: Condens. Matter* **3**, 69 (1991).